ARGO-YBJ Experiment: review of results on Gamma-Ray Astronomy and Cosmic Ray Astrophysics

R. Assiro [1] , P. Bernardini [1 2] , A. Corvaglia [1], P. Creti [1], A. D'Amone [1 2], I. De Mitri [1 2], G. Mancarella [1 2], G. Marsella [1 2] , D. Martello [1 2], M. Panareo [1 2], L. Perrone [1 2], C. Pinto [1 2], S. Sbano [1 2], A. Surdo [1]

[1]Istituto Nazionale di Fisica Nucleare, sez. di Lecce, Italy

[2]Dipartimento di Fisica, Università del Salento, Italy

1. Introduction

The ARGO-YBJ [1] experiment has been the only air shower array with a full-coverage active area operated at high altitude, with the aim of studying the cosmic radiation at an energy threshold of a few hundreds GeV. The large field of view ($\sim 2\,sr$) and the high duty cycle ($> 85\%$) allow a continuous monitoring of the sky in the declination band from -10° to 70° [2]. It stopped operation in February 2013.

Crucial requirements for ARGO-YBJ to perform such studies were the operation stability, the pointing accuracy and the angular resolution. The performance of the detector and the operation stability were continuously monitored by observing the Moon shadow, i.e. the deficit of cosmic rays (CR) detected in its direction. Indeed, the size of the deficit allows the measurement of the angular resolution, while its position allows the evaluation of the absolute pointing accuracy of the detector. In addition, positively charged particles are deflected towards East due to the geomagnetic field by an angle depending on energy: $\Delta\theta \sim 1.6^\circ Z/E[TeV]$. Therefore, the observation of the displacement of the Moon provides a direct calibration of the relation between shower size and primary energy. The Moon was observed with a sensitivity of about 9 standard deviations (s.d.) per month for events with a multiplicity $N_{pad} \geq 40$ and zenith angle $\theta < 50^o$ corresponding to a proton median energy $E_p \sim 1.8\,TeV$. The angular and energy resolutions are in good agreement with the expected values obtained by Monte Carlo analysis. In the energy range $(1-30)\,TeV$ the estimated energy uncertainty is smaller than 13%. The measured angular resolution is better than 0.5° for CR-showers of energies $E > 5\ TeV$ and is smaller by about $(30-40)\%$, depending on the multiplicity, for γ-rays due to the better defined time profile of the showers. The month analysis showed that the pointing accuracy was stable within 0.1^o while the angular resolution is stable at a level of 10%.

With all data from July 2006 to November 2010 ARGO-YBJ observed the CR Moon shadowing effect with a significance of about 70 s.d. (Fig. 1). The data analysis and a full account of the results are given in [3].

In the following sections the main results concerning gamma-ray source observations and cosmic ray astrophysics studies, achieved after about 3 years of data taking, are reviewed.

2. Gamma-Ray Astronomy

In ∼4 years of operation ARGO-YBJ has detected and monitored the Crab Nebula, the extended galactic sources MGRO J1908+06 and MGRJ2031+41, and the extragalactic sources

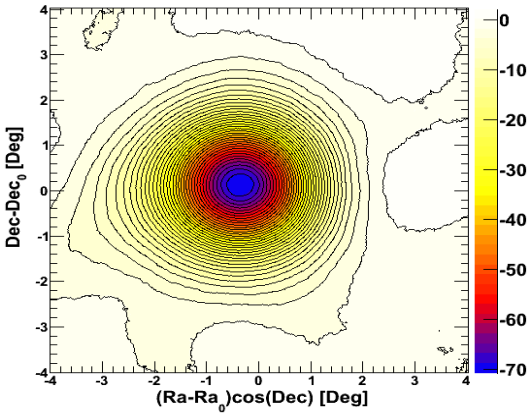

Figure 1. Moon shadow significance map for events with $N_{pad} \geq 40$ fired pads, observed by the ARGO-YBJ experiment in the period July 2006 - November 2010. The colour scale gives the deficit statistical significance in terms of s.d.

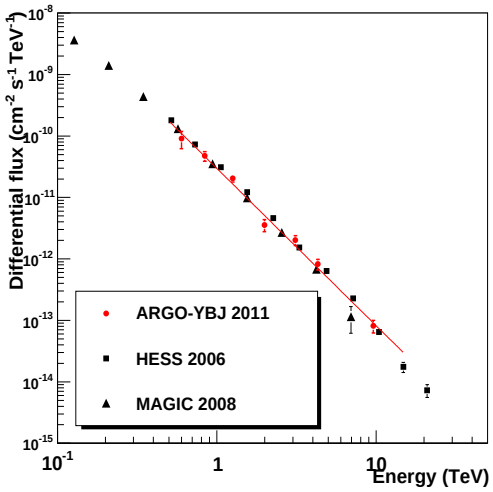

Figure 2. The Crab Nebula spectrum obtained by ARGO-YBJ, compared to measurements by other detectors.

Mrk 421 and Mrk501.

The spectrum of the Crab Nebula in the energy range 0.5-10 TeV is in good agreement with other experiments, showing the reliability of the ARGO-YBJ measurement, the stability of the detector and the accuracy of the analysis and simulation procedures (Fig. 2).

A search for possible TeV flares on timescales ranging from 1 to 20 days during a period of ∼3 years showed no statistical significant flux variations. A particular attention has been devoted to 4 time intervals in which a flaring emission has been observed at energies E > 100 MeV by satellite experiments[5]. In 3 out of 4 cases ARGO-YBJ detected an excess of events of ∼2.5-3 standard deviations in addition to the steady flux, in coincidence with the lower energy emission. The moderate statistical significance of the single observations are not enough to claim the detection, however the presence of a small signal in three flares, suggests the possibility of a flaring activity of the Crab Nebula also in the TeV region, that should be confirmed by other measurements.

For the extended sources MGRO J1908+06 and MGRO J2031+41 the measured flux are in agreement with the Milagro detector, but in both cases are larger than that reported by Cherenkov detectors. The origin of this disagreement is not yet clear (Fig. 3).

The blazar Mrk 421 underwent several active periods during our observation time, showing a high gamma ray flux variability. A strong correlation between gamma rays and X-rays has been observed over the whole observation period, with a hardening of both gamma and X-ray spectra during the flares. According to our analysis, the spectral behavior during the 4 different flux states is consistent with the expectations of the one-zone Synchrotron Self-Compton model (Fig. 4).

A similar analysis has been performed for Mrk501, that after a long quiet phase, underwent a flaring period where gamma rays of energy higher than 8 TeV have been detected. Because of this unusual emission of energetic photons, the observed SED cannot be satisfactorily described by the above SSC simple

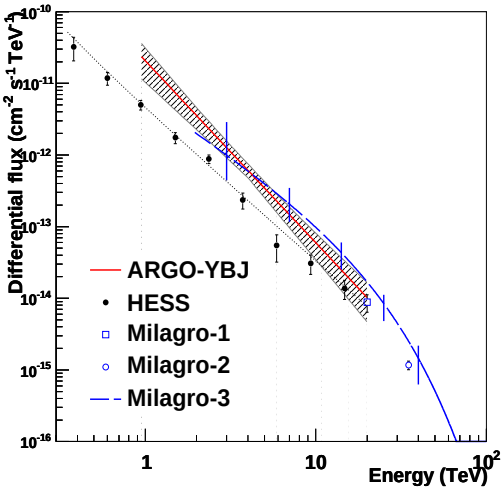

Figure 3. Gamma ray flux from MGRO J1908+06 measured by ARGO-YBJ and other detectors.

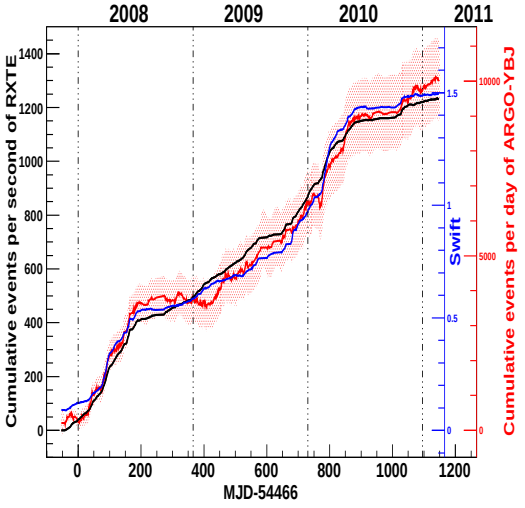

Figure 4. Cumulative light curves of Mrk 421. Red curve: ARGO-YBJ (the shaded region indicates one standard deviation statistical error); black curve: RXTE/ASM; blue curve: Swift/BAT, normalized to the RXTE/ASM curve.

model, that is consistent only with the data recorded during the quiet phase[6].

The results presented here have been obtained without any gamma-hadron discrimination. Methods to recognize and reject cosmic ray showers based on the different space-time distributions of the particles of the shower front with respect to gamma ray showers are currently under study [7,8] in order to increase the sensitivity of the detector.

3. Cosmic Ray Astrophysics

4. Interplanetary Magnetic Field measurement by Sun shadow

CRs arrive mostly isotropically at the Earth and can be recorded by detectors on ground. Those coming from the Sun direction are absorbed and form a clear deficit, a shadow, in a uniform sky map. The Interplanetary Magnetic Field (IMF) deflects the cosmic rays along their path to the Earth and shifts the Sun shadow from its true position. Its y-component, B_y, defined as lying in the ecliptic plane and perpendicular to the line of sight Sun-Earth, moves the Sun shadow in the north-south direction. At the YangBaJing site the geomagnetic field has a declination angle which is less than 0.5°, therefore it does not contribute to the north-south shift of the Sun shadow. Using this effect, ARGO-YBJ has measured B_y in the period July 2006 to October 2009, when the solar activity stayed at its minimum for an unexpectedly long time. This is a particularly good time window and fits the stability requirement of B_y. Indeed the IMF is better studied in a quiet phase of the Sun as it is strongly modulated by the solar activity. Using this data set, namely 903

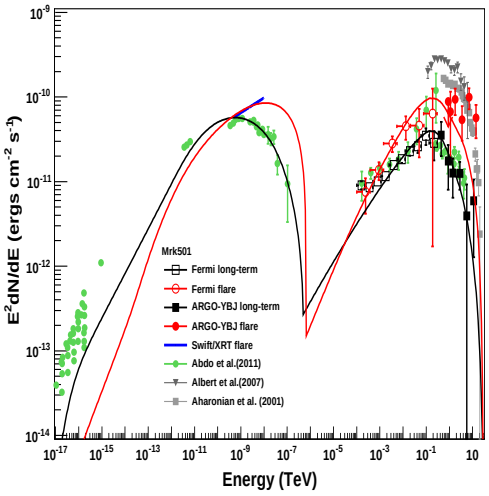

Figure 5. Spectral energy distribution of Mrk501. The solid lines represent the SEDs according to the SSC model for the quiet and active phases.

exposure days in total, the map of the Sun shadow has a maximum significance of 45 s.d. located at $(0.17 \pm 0.02)^\circ$ toward north and $(0.26 \pm 0.02)^\circ$ toward west. As confirmed by the moon shadow observation [12], the shift toward north represents a systematic effect while the westward one is exactly expected due to the geomagnetic effect. By fitting the measured Sun displacement as a function of the solar longitude, one can estimate B_y, with a minimal assumption on its model [13]. In simulating the Sun shadow displacement, the CR composition as measured by space/balloon born experiments has been assumed [14]. Data have been grouped in two sub-sample, namely G1 (January 2008 to April 2009) and G2, where G1 contains data with the IMF showing a bi-sector structure, while G2 is related to the 4-sector structure of the IMF.

Then the Sun shadow displacement has been plotted versus the solar longitude, or the Carrington period (27.3 days) which is the time we need to observe one complete Sun rotation, and finally the B_y value extracted according to the simple model in [13]. The results are shown in Fig.6: the solid curves, with uncertainty represented by the shaded area, are the results of the ARGO-YBJ experiment shifted by 21° while the solid dots represent the measurements by the orbiting detectors [15]. The B_y amplitudes measured in both cases by ARGO-YBJ are of the same order of magnitude, namely in the band of (2.0±0.2) nT; the two B_y profiles are consistent with the alternating periodical pattern and agree with the satellite measurements. The shift of 21°, corresponding to 1.6 days ahead, comes from a ray-tracing MC simulation used to track the primary particle pattern and is due to two causes: a) the speed difference between the solar wind (400 km/s), which transports the field, and the TeV particles ($\sim c$) that we measure; b) the bending of the primary particle trajectory by the IMF. Therefore, even more importantly, this measurement could foresee fluctuations of IMF which will sweep the Earth about 2 days later, provided the detector has the right sensitivity, so demonstrating a potential forecasting capability for magnetic storms due to solar events.

5. $\bar{p}/p$ ratio measurement by Moon shadow

As in the case of the Sun, a similar deficit of the cosmic ray flux is observed in the Moon direction. This effect can be used to estimate the $\bar{p}/p$ ratio in the primary CR flux. Fig.7 shows the statistical significance map of the Moon region [12]. With all data from July 2006 to December 2009 (about 3200 hours on-source in total) we observed the CR Moon shadowing effect with a significance of about 55 s.d.. Two ranges of pad multiplicity have been chosen for the antiproton abundance measurement, namely $40 \leq N_{pad} < 100$ and $N_{pad} \geq 100$.

In the former bin the statistical significance of the Moon shadow deficit is 34 s.d., the measured angular resolution is about 1°, the proton median energy is 1.4 TeV. In the latter multiplicity bin the significance is 55 s.d., the measured angular resolution about 0.6°, the proton median energy is 5 TeV and the number of missing events about 46500. The accuracy of the energy scale determination is estimated to be less than 18% in the rigidity range $1-30$ TeV/Z. Using all data collected until November 2009, we set two upper limits (see Fig.8) on the $\bar{p}/p$ flux ratio [16]: 5% at an energy of 1.4 TeV and 6% at 5 TeV with a 90% confidence level. In the few-TeV range the ARGO-YBJ results are the lowest available, useful to constrain models for antiproton production.

6. Anisotropy

Observation of the sidereal cosmic ray anisotropy at energies of 1 - 100 TeV is a useful tool for probing the magnetic field structure in our interstellar neighborhood as well as the distribution of sources. Cosmic-rays at these energies are almost entirely of Galactic origin and are expected to be nearly isotropic due to interactions with the Galactic magnetic field [22]. ARGO-YBJ has measured a large scale anisotropy [23] as shown in Fig.9 where three distinct regions, respectively labeled as I, II and III , are reported. The region I is the spread excess area called "Tail-in", which is composed of two small discrete regions with peak significance of about 20. s.d. and a relative intensity the order of 0.1%. Region II is a large deficit area, identified as "Loss-cone"; last, the excess in Region III, which is close to the Cygnus region. To quantify the scale of anisotropy the 1-dimensional R.A. projections of the 2-dimensional maps have been fitted with the first two harmonics at different energies. The preliminary results on amplitude (A_1) and phase ϕ_1 of the first harmonic, shown in Tab.1, are in good agreement with the results obtained by other experiments measuring atmospheric muons [24]. The heliosphere is suggested to be responsible for the "Tail-in" excess and the local interstellar MF for the "Loss-cone" deficit [25]. However, it is argued that the observation of multi-TeV anisotropy does not favour this interpretation, as the heliosphere cannot influence CRs with energy larger than 10 TeV [26,27]. The discrete distribution of cosmic-ray sources is another possible cause. Concerning the medium-scale anisotropy, the two anisotropy hot spots in Region I reported by Milagro at 10 TeV [28], have been observed, at 2 TeV, also by the ARGO-YBJ detector. The two excesses (Fig. 10) have significance greater than 10 s.d. and correspond to a flux increase of about 0.1%. The origin of these anisotropy regions is not understood yet.

E (TeV)	A_1	ϕ_1 (°)
0.9	$(6.12 \pm 0.11) \cdot 10^{-4}$	(42.2 ± 1.0)
1.5	$(7.92 \pm 0.14) \cdot 10^{-4}$	(31.8 ± 1.0)
2.4	$(9.84 \pm 0.22) \cdot 10^{-4}$	(37.0 ± 1.3)
3.7	$(10.43 \pm 0.27) \cdot 10^{-4}$	(28.4 ± 1.5)
7.2	$(11.61 \pm 0.37) \cdot 10^{-4}$	(29.2 ± 1.8)
12.5	$(8.73 \pm 0.55) \cdot 10^{-4}$	(37.0 ± 3.6)
23.6	$(3.82 \pm 0.49) \cdot 10^{-4}$	(7.8 ± 7.3)

Table 1
Values of amplitude and phase of the first harmonic from the fit of the 1-dimensional R.A. projection at different energies.

7. Measurement of the light component of CRs in the 5-200 TeV region

By using a Bayesian approach, a measurement of the light-component spectrum of the primary CRs, in the energy region (5 - 200) TeV, has been performed [29]. The energy spectrum was obtained through a Bayesan unfolding procedure [30] applied to the ARGO-YBJ data collected in the period January - May 2008. A full detector simulation was performed in order to evaluate the relevant quan-

tities needed by the unfolding procedure. The results are shown in Fig.11. The measured spectrum refers to the energy region 5 - 200 TeV. The results are affected by a statistical error of the order of 1%. Sources of systematic errors taken into account in the analysis were: a) the selection cuts on the measured quantities; b) the uncertainties of the detector response; c) effects related to the the fraction of the helium component used to evaluate the Bayesian probabilities. We estimated the result to be affected by a total uncertainty of the order of 10% The contribution of elements heavier than helium nuclei to the energy spectrum has been estimated to be negligible. The results have been compared both to the recent results of the CREAM experiment [14] and to the best fit provided by Horandel for the proton and helium experimental fluxes [31]. The point at 80 TeV represents the "p + He" intensity measured by the EAS-TOP and MACRO experiments [32], at the Gran Sasso Laboratory, by combining the quantities simultaneously measured by different detectors, namely the electromagnetic component of the shower, the Cerenkov light and the high energy muons. As can be seen, the ARGO-YBJ data are in agreement with the recent CREAM measurement.

8. Measurement of the proton-Air cross section

ARGO-YBJ has performed a measurement of the proton-air cross section by exploiting the attenuation of the CR flux with the increasing of zenith angles θ (i.e., atmospheric depth) [33]. At fixed primary energy and shower age, the flux goes like $I(\theta) \simeq I(0) exp(-h_{0'}(sec\theta - 1)/\Lambda_{obs})$, where $h_{0'}$ is the vertical atmospheric depth at the detector location and Λ_{obs} is related to the mean free path λ_{int} of the primary particle through the parameter $k = \Lambda_{obs}/\lambda_{int}$. This parameter, which takes into account the fluctuations both in the shower development and in the shower sampling, is calculated via MC simulation and has a small dependence on the hadronic interaction models in the considered energy region. Energy and shower maximum position have been fixed by using the specific features of the ARGO-YBJ detector (see [33] for details) and five energy bins have been considered in the range $1 - 100$ TeV. The measured p-air cross section is plotted in Fig.12; the p-p total cross section, estimated by applying the Glauber theory, is shown in Fig.13.

9. Approaching higher energies with the Analog Readout

The RPC charge readout [34,35], which has been in operation on the entire central carpet since December 2009, extends the energy range of measurement, allowing the study of the cosmic radiation up to PeV energies. Fig.14 shows a shower as seen by the analog readout system. In the vertical scale is the number of particles measured in each BigPad, whose area is about 1.7 m^2. According to MC simulations, the shower should be initiated by a proton primary of about 2 PeV. We stress that no experiment has ever measured the shower core with such a detail. Owing to the analog readout, the measurement of the proton-air cross section and the composition studies will be extended to PeV energies. The differential rate of the measured particle number at the shower core (PMax) is shown in Fig.15; the two colors refer to two different full scales of operation of the system. To obtain this spectrum, events with core in a fiducial area of the central carpet (the 6×9 central clusters, corresponding to 2380 m^2) and zenith angle $\theta \leq 15^\circ$ have been selected. PMax has a good correlation to the number of particles measured within 10 meters around the shower core, which in turn relates to the primary energy and to the primary mass. In the small upper-right square the MC expectation for PMax is reported, with respect to the primary energy, for three different primaries, namely proton, Helium and Iron.

REFERENCES

1. R. Assiro *et al*, Annual Reports (*ARGO-YBJ Experiment in Tibet*) 2008 and 2010.
2. B. Bartoli *et al* (ARGO-YBJ Coll.), NIM A, vol. 659, 428-433 (2011).
3. B. Bartoli *et al* (ARGO-YBJ Coll.), Phys. Rev. D, vol. 84, 022003 (2011).
4. G. Aielli *et al* (ARGO-YBJ Coll.), The Astrophysical Journal, **714**: L208 (2010).
5. M.Tavani et al., Science 331 (2011) 736.
6. B.Bartoli et al. ApJ 758 (2012) 2.
7. A.Pagliaro et al. 2011, Proc.32nd ICRC, Beijing, China (2011) HE1.1.
8. M.Iacovacci et al. 2011, Proc. of SciNeGHE Conference, Lecce, Italy (2012).
9. A.A. Abdo *et al.*, Physical Review Letters, **101** (2008) 221101-(1-5)
10. G. Aielli, et al., 2006, Nucl. Instr. and Meth. A, 562, 92
11. Aielli, G., et al., 2009, NIM A, 608, 246.
12. Bartoli, B. et al., 2012, Phys. Rev. D, 84, 022003.
13. Amenomori, M., et al., 2000, ApJ, 541, 1051.
14. Ahn, H.S., et al., 2010, ApJ , 714, L89.
15. King, J.H. and Papitashvili, N. E., 2004, J. Geophys. Res., 110, A02209, 10.1029/2004JA 010804; corresponding data are available at http://omniweb.gsfc.nasa.gov/
16. Bartoli, B. et al., 2012, Phys. Rev. D, 85, 022002.
17. F. Donato et al., 2009, Phys. Rev. Lett. 102, 071301.
18. S. A. Stephens and R. L. Golden, 1987, Space Sci. Rev. 46, 31.
19. S. A. Stephens, 1985, Astron. Astrophys. 149, 1.
20. M. Cirelli et al., 2009, Nucl. Phys. B813, 1.
21. P. Blasi and P. D. Serpico, 2009, Phys. Rev. Lett. 103, 081103.
22. Berezinskii, V. S., Bulanov, S. V., Dogiel, V. A., and Ptuskin, V. S. 1990, Astrophysics of Cosmic Rays (Amsterdam: North-Holland).
23. Cui, S.W., et al. for the ARGO-YBJ Coll., ICRC2011 - Beijing, HE1.1, n.0041.
24. Guillian, G., et al., 2007, Phys. Rev. D, 75, 062003.
25. Nagashima, K., et al., 1998, Journal of Geophysical Res.,103,17429.
26. Amenomori, M., et al., 2006, Science, 314, 439.
27. Hall, D.L., et al., 1999, JGR 104, 6737.
28. Abdo, A.A., et al., 2008, Physical Review Letters, 101, 221101.
29. Bartoli, B. et al., 2012, Phys. Rev. D, 85, 092005.
30. D'Agostini, G., 1995, Nucl. Instrum. Meth. A, 362, 487.
31. Horandel, J.R., 2003, Astropart. Phys., 19 193.
32. Aglietta, M., et al., 2004, Astropart. Phys., 21, 223.
33. G.Aielli et al., 2009, Phys. Rev. D, 80, 092004.
34. S. Mastroianni, M.Iacovacci, et al., 2011, Nuclear Science, IEEE Transactions 581838-1844
35. M. Iacovacci, S. Mastroianni for the ARGO-YBJ Coll., ICRC2011 - Beijing, HE1.1, n.1028

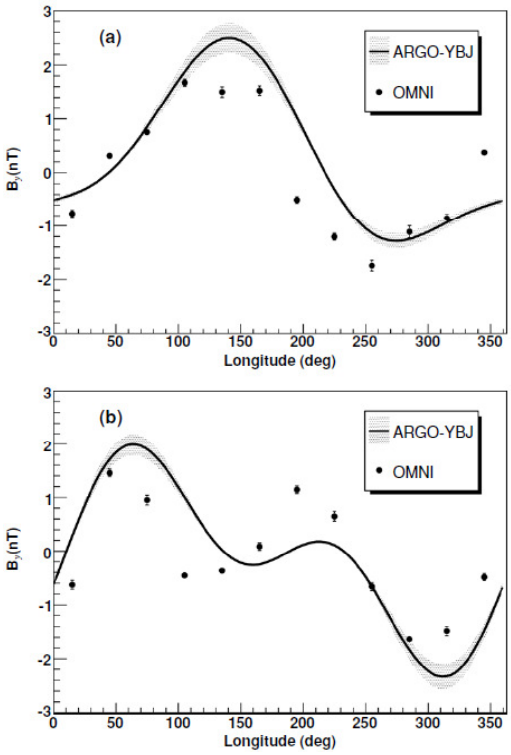

Figure 6. The solid curve represents the B_y component of IMF field as measured by the ARGO-YBJ near the Earth; the shaded area corresponds to an uncertainty of one standard deviation. In the upper panel a), corresponding to period G1 (see text), a clear bisector pattern is observed. The solid dots represent the measurements using the OMNI observational data downloaded from [15]. In the lower panel b), the results with the 4-sector structure in period G2 are displayed. In both cases a phase shift of 21° (see text) is applied to the ARGO-YBJ profile.

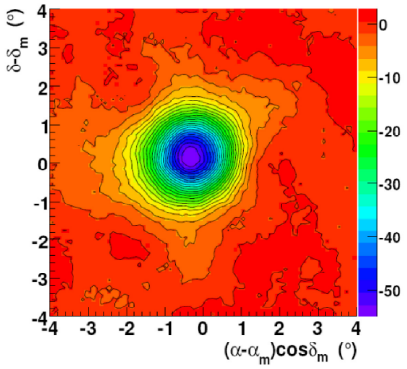

Figure 7. Moon shadow significance map for events with $N_{pad} \geq 100$ fired pads. The coordinates are R.A. α and DEC. δ centered on the Moon position (α_m, δ_m). The color corresponds to the statistical significance according to the color scale on the right, where the correspondence is with the number of s.d..

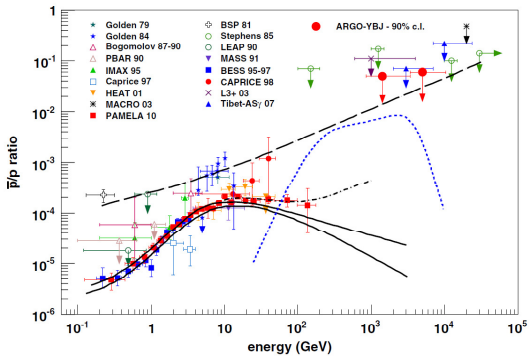

Figure 8. The antiproton to proton flux ratio obtained with the ARGO-YBJ experiment compared with all the available measurements. The solid curves define the propagation uncertainty band for a pure secondary production of antiprotons during the CR propagation in the Galaxy [17], while the long-dashed line refers to a model of extragalactic primary $\bar{p}/p$ production [18,19]. The dotted line refers to the contribution of antiprotons from the annihilation of a heavy dark matter particle [20]. The short-dashed line shows the calculation by Blasi and Serpico [21] for secondary antiprotons including an additional $\bar{p}/p$ component produced and accelerated at CR sources.

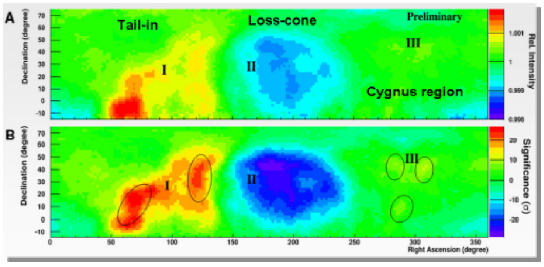

Figure 9. Large scale cosmic-ray anisotropy observed by ARGO-YBJ at energies of $\sim$ 2 TeV . In the upper plot the colour scale gives the relative CR intensity, in the lower plot the statistical significance in standard deviations.

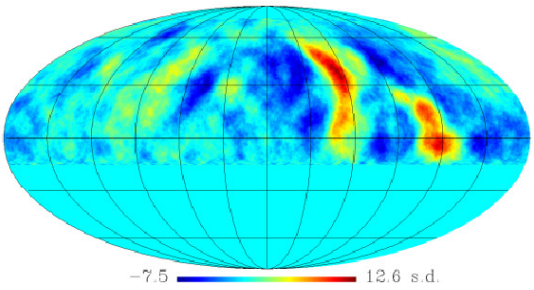

Figure 10. Medium scale anisotropy of cosmic-rays at energies $\sim$ 2 TeV as measured by ARGO-YBJ. The color scale gives the statistical significance in standard deviations.

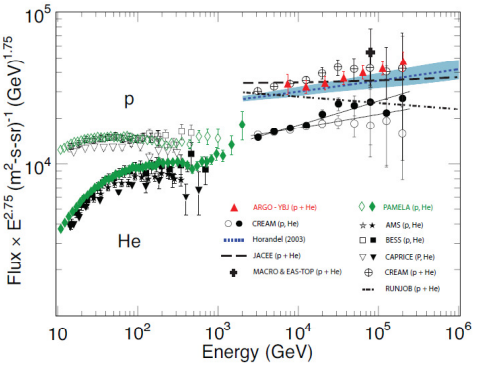

Figure 11. The differential energy spectrum of the light-component (proton and helium) measured by ARGO-YBJ (filled triangles) compared to the proton spectrum (open circles) and helium spectrum (filled circles) measured by the CREAM experiment [14].

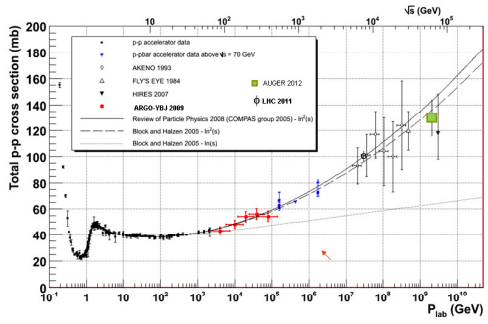

Figure 13. Total p-p cross section, obtained by ARGO-YBJ starting from the p-air cross section; also results published by other CR experiments as well as accelerator experiments are shown.

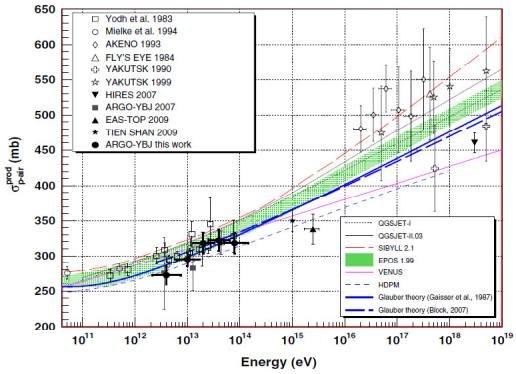

Figure 12. Proton-air production cross section measured by ARGO-YBJ and by other CR experiments (see [33]). Also shown are the predictions of two different calculations based on Glauber theory. In this plot ARGO-YBJ points have been already corrected for the effects of CR primaries heavier than protons.

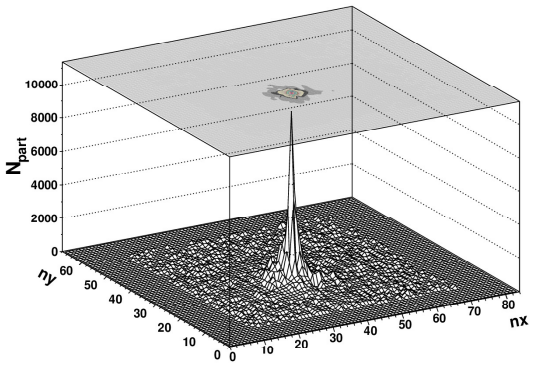

Figure 14. Shower as recorded by ARGO-YBJ through the analog readout system. According to MC simulations, the shower would correspond to a primary proton of about 2 PeV. In the vertical scale is the number of particles measured in each BigPad, whose area is about 1.7 m^2; nx and ny are the coordinate of the BigPad.

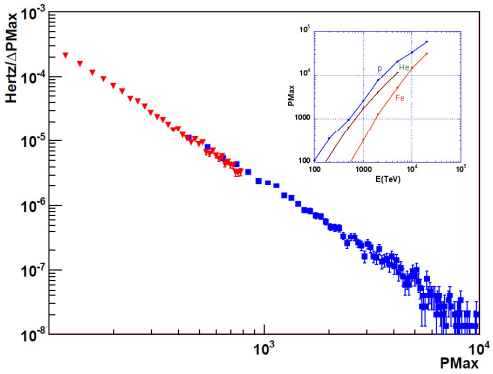

Figure 15. Differential rate of the particle number at the shower core (PMax) for events with core in a fiducial area of the carpet (2380 m^2) and $\theta \leq 15°$. In the small upper-right square square the MC expectation for PMax is reported with respect to the primary energy for three different primaries, namely proton, Helium and Iron.